CRYSTAL GROWTH & DESIGN

Article

Cite This: *Cryst. Growth Des.* 2018, 18, 954–961

pubs.acs.org/crystal

Opening Pandora's Box: Chirality, Polymorphism, and Stoichiometric Diversity in Flurbiprofen/Proline Cocrystals

Natalia Tumanova,[†] Nikolay Tumanov,[‡] Koen Robeyns,[†] Franziska Fischer,[§] Luca Fusaro,[‡] Fabrice Morelle,[†] Voraksmy Ban,[∥] Geoffroy Hautier,[†] Yaroslav Filinchuk,[†] Johan Wouters,[‡] Tom Leyssens,*[,†] and Franziska Emmerling*[,§]

[†]IMCN Institute of Condensed Matter and Nanosciences, Université catholique de Louvain, Place Louis Pasteur 1, 1348 Louvain-la-Neuve, Belgium

[‡]Chemistry Department, University of Namur, Rue de Bruxelles 61, 5000 Namur, Belgium

[§]BAM Federal Institute for Materials Research and Testing, Richard-Willstätter-Strasse 11, 12489 Berlin, Germany

[∥]MS-Group, Swiss Light Source, Paul Scherrer Institute, 5232 Villigen PSI, Switzerland

Supporting Information

ABSTRACT: Proline has been widely used for various cocrystallization applications, including pharmaceutical cocrystals. Combining enantiopure and racemic flurbiprofen and proline, we discovered 18 new crystal structures. Liquid-assisted grinding proved highly efficient to explore all the variety of crystal forms. A unique combination of state-of-the-art characterization techniques, comprising variable temperature *in situ* X-ray diffraction and *in situ* ball-milling, along with other physicochemical methods and density functional theory calculations, was indispensable for identifying all the phases. Analyzing the results of *in situ* ball-milling, we established a stepwise mechanism for the formation of several 1:1 cocrystals via an intermediate 2:1 phase. The nature of the solvent in liquid-assisted grinding was found to significantly affect the reaction rate and, in some cases, the reaction pathway.

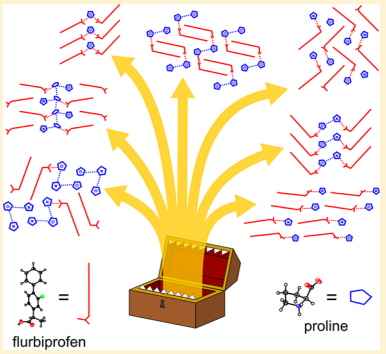

INTRODUCTION

Mechanochemistry has grown to a versatile synthesis approach to obtain known or new organic compounds. Compared to conventional, solution-dependent chemistry, the method is inherently environmentally friendly avoiding solvents and limiting waste in additional cleaning steps. Among the intensively studied organic materials, pharmaceutical cocrystals are considered good alternatives to existing drug formulations as they allow modifying pharmacological properties without affecting the chemical integrity of drugs.[1−6] Amino acids are natural to the body, and thus their application as cocrystal formers offers a possibility to produce safer drugs with better therapeutic performance.

Chiral drugs may respond differently when cocrystallized with chiral coformers,[7] which offers new alternatives for chiral resolution techniques.[8,9] Studying cocrystals from chiral active pharmaceutical ingredients (APIs) in combination with chiral coformers not only presents an opportunity for the potential improvement of the drug's performance, but also helps gaining insight into challenges and pitfalls of chiral cocrystallization, which is crucial for the design, development, and control of chiral cocrystals for industrial applications.

Herein, we focus on the flurbiprofen/proline (**flu**/**pro**) system. This model system allows studying both the structural peculiarities and the chirality in cocrystals. Moreover, cocrystallization of **flu** with amino acids may be another alternative way to improve its therapeutic performance. **Flu** is a nonsteroidal anti-inflammatory drug poorly soluble in water; it has already been subjected to cocrystallization to improve its mechanical properties, dissolution performance, and hygroscopicity.[10] **Pro** seems to be a promising coformer for various cocrystal applications. Cocrystals of dapagliflozin, a drug used to treat type II diabetes, with **pro** have been patented.[11] There are examples of **pro** cocrystals with naproxen, a nonsteroidal anti-inflammatory drug[12] and with β-C-arylglucoside, another promising compound to treat diabetes.[13] L-**pro** has found application in chiral resolution through diastereomeric salt or cocrystal formation.[14−16] It was also studied in relation to conformational polymorphism[17] and applied to create an amino acid derived semiconductor.[18] **Pro** was found to easily form cocrystals or salts with carboxylic acids;[19−26] for instance, its tartrate may be considered as a material for nonlinear optical applications,[27] as well as boronic acids.[28,29]

This work illustrates how combining enantiopure and/or racemic forms of **flu** and **pro** results in a rich variety of molecular crystals, 18 in total, including polymorphs, stoichiometrically diverse forms, solvates, and a new polymorph of L-**pro**. The focus was set on the mechanochemical preparation of

Received: October 13, 2017
Revised: January 2, 2018
Published: January 4, 2018

DOI: 10.1021/acs.cgd.7b01436
Cryst. Growth Des. 2018, 18, 954–961

cocrystals. The products of mechanochemical reactions may often represent complicated mixtures of various products not easily analyzable especially when the phases are unknown. We show how combining state-of-the-art X-ray diffraction techniques with other physicochemical methods helps in identifying phases and untangling problematic cases.

EXPERIMENTAL SECTION

A description of some of the experimental procedures is given here; the Supporting Information provides experimental details on structure determination and density functional theory (DFT) calculations.

Materials. All compounds used in this work were purchased from Sigma-Aldrich and used without further purification. Commercial racemic **flu** was identified as the $P\bar{1}$ polymorph, CCDC REF FLUBIP.[30]

Laboratory Liquid-Assisted Grinding. **R-flu** was screened with a series of amino acids by liquid-assisted grinding; the compounds were mixed in a 1:1 ratio (~50 mg of powder in total, 5 μL of MeOH) in 2 mL Eppendorf tubes and put into a Retsch MM400 mixer mill for 60 or 90 min at a frequency of 30 Hz. Table S1.1 lists all the amino acids used. Positive hits were found only for L- and D-**pro**.

Further liquid-assisted grinding with five different solvents, methanol, ethanol, acetonitrile, isopropanol, and water (~50−100 mg of powder in total, 3−10 μL of solvent, 25−90 min, 30 Hz, 1:1, 2:1, 1:2 ratios; a 1:3 ratio was additionally used for the ***R*-flu**/L-**pro** combination) was performed for various combinations of enantiopure and racemic **flu** and **pro**.

Resultant powders were analyzed by powder X-ray diffraction (CuKα radiation, λ = 1.5418 Å) using a Siemens D5000 diffractometer (2θ was scanned from 2 to 50° with a step of 0.02°) or a X'pert PRO PANalytical diffractometer (2θ was scanned from 4.022 to 49.990° with a step of 0.017°). Diffraction patterns of pure phases were simulated using the Mercury[31] software; the structures of L-proline (CCDC PROLIN[32]), L-proline monohydrate (CCDC RUWGEV[33]), DL-proline (CCDC QANRUT[34] and QANRUT01[35]), DL-proline monohydrate (CCDC DLPROM01[36]), and *RS*-flurbiprofen (CCDC FLUBIP[30] ($P\bar{1}$) and FLUBIP02[37] ($P2_1/n$)) were taken from the Cambridge Structural Database.[38]

Tables S2.1 and S2.2 and S2.4, S2.5, S2.6, and S2.7 summarize all liquid-assisted grinding experiments and their outcomes along with the information on how the samples were analyzed.

Diffraction data of selected powder samples were measured using a synchrotron radiation source. The structure determination from powder diffraction data is described in the Supporting Information.

The production of single crystals for X-ray diffraction, the data collection and structure determination are described in detail in the Supporting Information.

***In Situ* Variable Temperature Synchrotron X-ray Diffraction Data Collection.** Selected powders obtained by liquid-assisted grinding were packed into 0.5 mm glass capillaries and measured upon heating at a rate of 2 °C/min. All powder diffraction data, except *in situ* experiment for the **1:3 *R*-flu**/L-**pro** sample, were collected at MS-X04SA beamline at the Swiss Light Source (SLS) (PSI, Switzerland) equipped with a one-dimensional (1D) microstrip detector MYTHEN II. The measurements were performed at λ = 0.77494, 0.77663, 0.62173, 0.708 Å with a step of 0.0036°. The wavelength was calibrated using a standard NIST 640d Si sample. The **1:3 *R*-flu**/L-**pro** sample (sample 10 in Table S2.1) was measured *in situ* upon heating (2 °C/min) at the Swiss-Norwegian beamline BM1A at the European Synchrotron Radiation Facility (ESRF) (Grenoble, France), using a PILATUS 2M hybrid pixel detector at a wavelength of 0.7458 Å.

***In Situ* Ball-Milling Synchrotron X-ray Diffraction Data Collection.** *In situ* ball-milling X-ray diffraction experiments were performed at the μSpot beamline (BESSY II, Helmholtz Centre Berlin for Materials and Energy, Germany) using a Pulverisette 23 (Fritsch, Germany) ball mill and Perspex jars; the frequency was 50 Hz. Compounds were mixed and the solvent was added right before the experiment, except one sample for ***RS*-flu**/L-**pro** which, due to technical issues, was in contact with solvent for 2 h before being ground. Details for each experiment (duration of milling, amount of solvent, amounts of initial compounds) are summarized in Table S1.2. A beam diameter of 100 μm at a photon flux of 1×10^9 s^{-1} at a ring current of 100 mA was used. The experiments were performed at a wavelength of 1.000 Å using a double crystal monochromator Si (111). The spot size on the sample was 200 μm. Scattered intensities were collected with a two-dimensional X-ray detector (MarMosaic, CCD 3072 × 3072 pixels, pixel size 73 μm). Measurements were carried out every 30 s with a delay time of 3 or 4 s between two measurements. Obtained two-dimensional diffraction images were integrated (2θ vs intensity) using the program Fit2D.[39] Diffraction patterns were background corrected and plotted as a two-dimensional (2D) film representation using the Powder3D program.[40]

Differential Scanning Calorimetry (DSC) and Thermogravimetric Analysis (TGA). DSC curves were measured using a DSC 821 Mettler Toledo instrument. Prior to measurements, the instrument was calibrated using indium. Standard 40 μL aluminum crucibles were used. The heating rate was 2 °C/min over the range from 25 to 200−250 °C. TGA was performed using a TGA/SDTA 851 Mettler Toledo instrument. Samples were put into open aluminum oxide crucibles annealed at 1100 °C. The heating rate was 2 °C/min over a range from 25 to 350 °C. All experiments were carried out under nitrogen atmosphere (a flow rate of 50 mL/min). DSC data for pure ***R*-flu**, L-**pro pol I**, DL-**pro**, and ***RS*-flu** ($P\bar{1}$) are illustrated in Figures SA2.13, SA2.14, SA2.37, and SA2.51.

Solid-State NMR. ^{15}N NMR spectra were recorded at room temperature on a Bruker Avance-500 spectrometer operating at 11.7 T (50.6 MHz for ^{15}N) using a 4 mm CP-MAS Bruker probe. The sample was packed in a 4 mm zirconia rotor and measured with a spinning frequency of 15 kHz. ^{15}N CP-MAS spectra were recorded using the following acquisition parameters: 5 s relaxation delay, 2.6 μs (90°) excitation pulse, 2 ms contact time, 50 ms acquisition time. The processing comprised exponential multiplication of the free induction decay with a line broadening factor of 1 Hz, zero-filling, Fourier transform, phase and baseline corrections. The chemical shift scale was calibrated at room temperature with respect to a sample of solid NH_4Cl (39.3 ppm).[41] SS-NMR was used to confirm the ratio of the components in the **1:3 *R*-flu**/L-**pro** cocrystal. The spectra are presented in Figure S2.7.

Scanning Electron Microscopy (SEM). SEM images were obtained using a scanning electron microscope ZEISS SUPRA 40 equipped with a thermal field emission cathode (Schottky-emitter, ZrO/W-cathode). The acceleration voltage was set to 10 kV, and the working distance was between 5.9 mm and 6.3 mm. The images were adapted with an In-lens secondary electron detector, a SE2 secondary electron detector, and a QBSD backscatter detector. In addition, the scanning electron microscope is equipped with the energy dispersive X-ray spectrometers Thermo NSS (SiLi 5665) and Bruker X-Flash 5010 3403, Quantax 400.

RESULTS AND DISCUSSION

Preliminary screening of **flu** with a series of amino acids yielded cocrystals only with pro (see Table S1.1 for the list of amino acids used). The idea that not all the compounds readily cocrystallize even if they possess necessary hydrogen bonding groups is not new.[42−44] In our case, the reason may lie in the structural features of amino acids: the latter tend to form strong charge-assisted hydrogen bonds that can lead to strong stable structures.[45] In order for a cocrystal to be stable at certain conditions, the interactions in its structure should be compatible with those in the initial compounds. Thus, the absence of cocrystal formation with amino acids, other than proline, may be due to their failure to provide a hydrogen bond network competitive enough to the structures of pure amino acids.

Further, we set to investigate in more detail the following five combinations of **flu** and **pro** in order to identify new cocrystal

DOI: 10.1021/acs.cgd.7b01436
Cryst. Growth Des. 2018, 18, 954−961

Scheme 1. Schematic Representation of All the Cocrystal Forms Found for Each flu/pro Combination and of the Characterization Methods Used

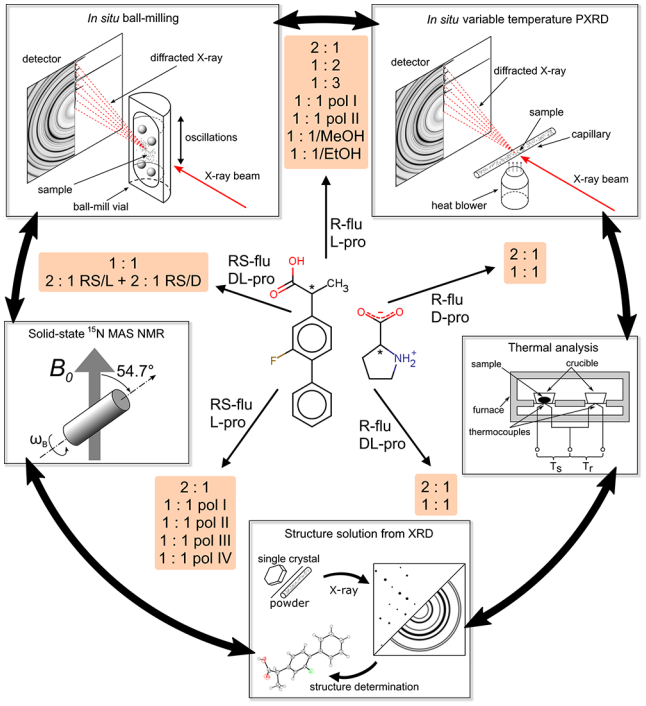

forms and to study chirality aspects of cocrystallization: ***R*-flu/L-pro (R/L)**, ***R*-flu/D-pro (R/D)**, ***R*-flu/DL-pro (R/DL)**, ***RS*-flu/L-pro (RS/L)**, and ***RS*-flu/DL-pro (RS/DL)**. We focused on liquid-assisted grinding (LAG), resorting to solution cocrystallization only to produce single crystals. The reasons were the following: (1) LAG is considered a "green" synthesis approach as it requires only small amounts of solvent as compared to conventional crystallization approaches; (2) LAG allows rapidly obtaining relatively pure materials; (3) the choice of solvents is not limited to those in which the initial compounds exhibit congruent behavior in solution, which is desired for effective solution cocrystallization; (4) in contrast to solution crystallization where thermodynamics play a substantial role, mechanochemical reactions depend to a higher extent on kinetic factors and may yield a wider variety of products not readily available from solution.[46−50] We chose five different solvents for LAG: methanol (MeOH) and ethanol (EtOH) in which both **flu** and **pro** are relatively well soluble (which would correspond to a congruent behavior if working in solution); isopropanol (ISPN) and acetonitrile (ACN), in which only **flu** is well soluble (incongruent behavior in solution); and finally water, in which only **pro** is well soluble (incongruent).

Scheme 1 shows that each combination in the **flu/pro** system resulted in multiple cocrystal forms. Since mechanochemical reactions may often result in complex mixtures of various products, identifying each phase required a unique combination of characterization techniques, including state-of-the-art *in situ* synchrotron X-ray diffraction methods, such as *in situ* ball-milling and *in situ* measurements upon variable temperature.

Laboratory powder X-ray diffraction (PXRD) allowed detection of new potential cocrystal phases. DSC and TGA helped identify systems with a complex behavior upon heating. Single-crystal XRD was essential for solving the crystal structures. Variable temperature synchrotron XRD complemented DSC and TGA data providing direct monitoring of phase changes upon heating. Synchrotron XRD data were indispensable for structure solution from powder data. Solid-state NMR was used to find the ratio between the cocrystal components in the **1:3 R/L** phase needed for its structure solution from PXRD. *In situ* ball-milling provided insight into LAG reactions, revealing intermediates and showing the solvent's influence on the process. DFT-d calculations were used to validate the structures found from PXRD (for structure validation see Supporting Information). Below we will discuss the most interesting findings of this work, illustrating them by the examples; detailed results on each **flu/pro** combination can be found in Supporting Information.

Even though simultaneous acquisition of synchrotron XRD data *in situ* upon varied temperature is common in inorganic chemistry,[51] its application to organic compounds for structure solution is less widespread. In this work, this method proved vital for untangling complicated cocrystal mixtures obtained after LAG, especially, when the phases were initially unknown:

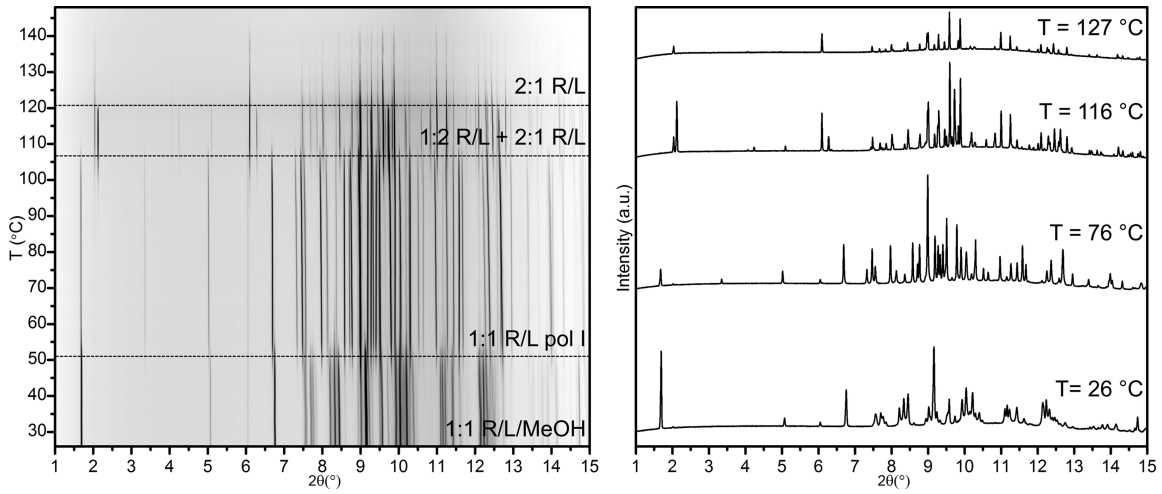

Figure 1. PXRD patterns measured *in situ* upon heating (from 26 to 150 °C, 2 °C/min) for the **R/L** sample prepared by 1:1 MeOH−LAG (sample 1 in Table S2.1), λ = 0.77494 Å: (left) film representation; (right) XRD patterns at selected temperatures: T = 26 °C − **1:1 R/L/MeOH**; T = 76 °C − **1:1 R/L pol I**; T = 116 °C − **2:1 R/L** and **1:2 R/L**; and T = 127 °C − **2:1 R/L**.

DOI: 10.1021/acs.cgd.7b01436
Cryst. Growth Des. 2018, 18, 954−961

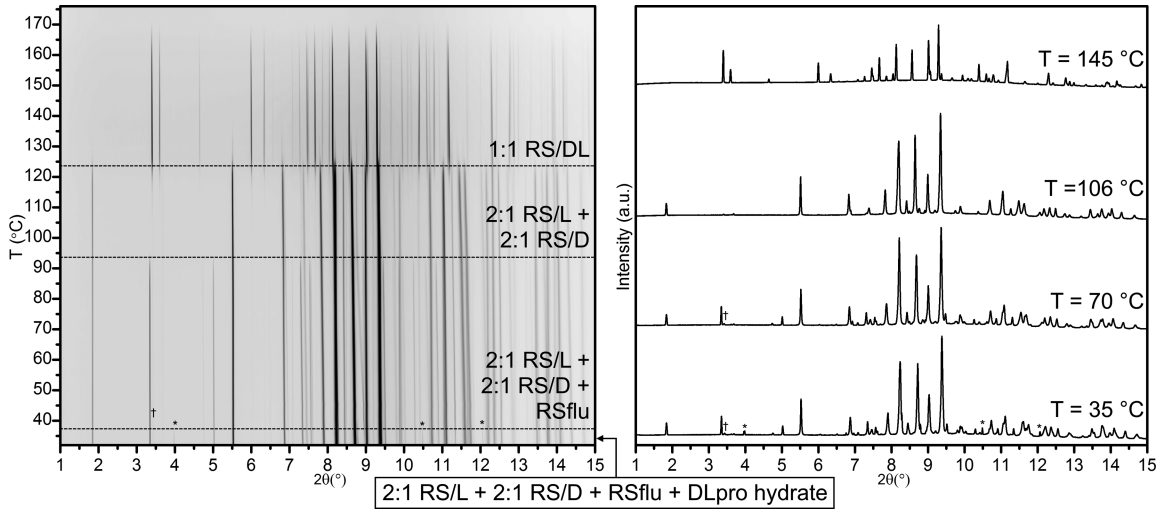

Figure 2. PXRD patterns measured *in situ* upon heating (from 35 to 177 °C, 2 °C/min) for the **RS/DL** sample prepared by 2:1 ISPN-LAG, λ = 0.708 Å: (left) film representation; (right) XRD at selected temperatures (sample 8 in Table S2.7): (a) T = 35 °C − ***RS*-flu**, (**2:1 RS/L** + **2:1 RS/D**), **DL-pro hydrate** (marked as "*"), and **1:1 RS/DL** (marked as "†"); T = 70 °C − ***RS*-flu**, (**2:1 RS/L** + **2:1 RS/D**), and **1:1 RS/DL**; T = 106 °C − (**2:1 RS/L** + **2:1 RS/D**) and **1:1 RS/DL**; T = 145 °C − **1:1 RS/DL**.

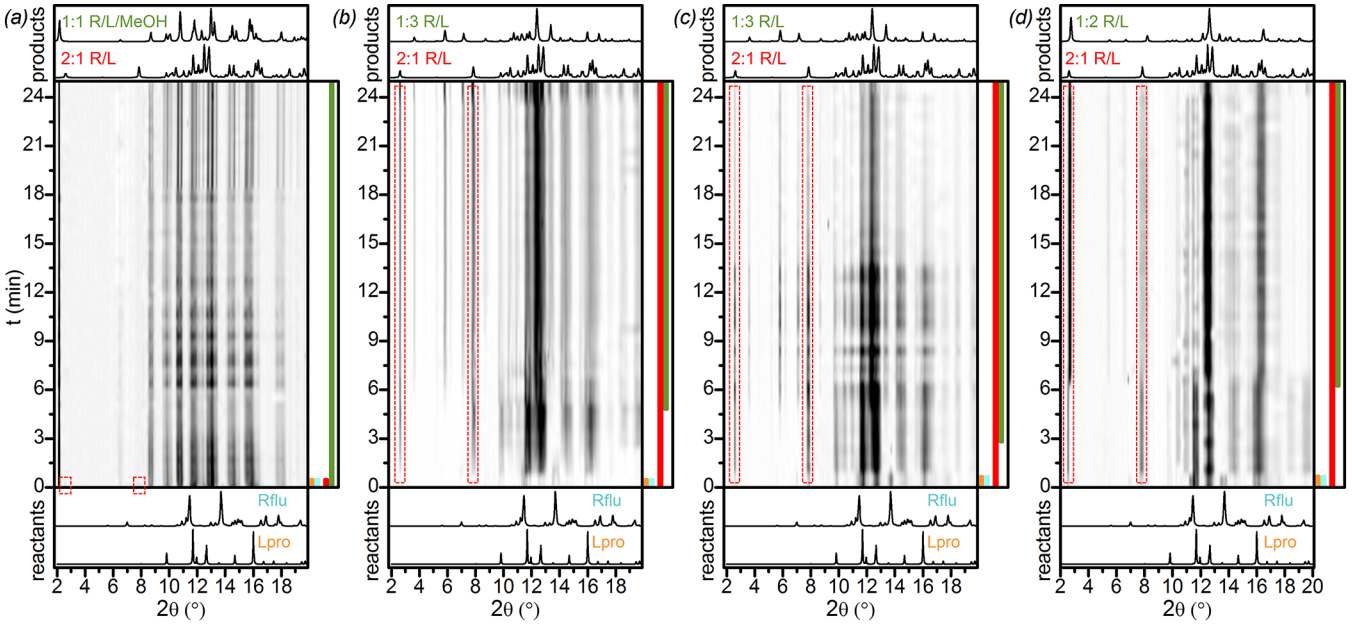

Figure 3. *In situ* ball-milling PXRD patterns for the **R/L** system, 1:1 ratio, λ = 1 Å: (a) MeOH-, (b) EtOH-, (c) ISPN-, and (d) ACN-LAG. Colored bands on the right side of each image represent the presence of phases; red dashed line indicates two the most representative peaks of the 2:1 phase.

beyond allowing direct monitoring of phase changes with temperature, it gave access to the XRD patterns of pure compounds. Owing to these data, we determined the structures of several new forms observed only at high temperatures: **L-pro pol II**, **1:1 R/L pol I**, **1:1 R/L pol II**, and **1:1 RS/L pol III**.

Figure 1 presents *in situ* data collected for the **R/L** sample produced by MeOH-LAG: the initial sample contained **1:1 R/L/MeOH**, which after solvent removal upon heating transformed into **1:1 R/L pol I**; upon further heating the **1:1 R/L pol I** phase disappeared followed by the emergence of a mixture of the **2:1** and **1:2 R/L** phases; the **1:2 R/L** phase melted first, leaving only the **2:1** phase.

In the **RS/DL** system, *in situ* variable temperature PXRD data helped us to prove the conglomerate formation (Figure 2), which was suspected but not entirely obvious due to the impurities in the sample. Uncertainty arose from the fact that in the **RS/DL** system, any of the **2:1** combinations could have emerged, and all of them have similar XRD patterns, not easily distinguishable with laboratory PXRD (Figure S2.53). Hence, *in situ* PXRD upon variable temperature was essential to confirm the presence of the (**2:1 RS/L** + **2:1 RS/D**) conglomerate as it gave access to its pure XRD pattern.

Another finding was a phase crossover observed in the **1:1 R/DL** system upon heating, illustrated in Figure S2.24.

In situ monitoring of ball-milling reactions by X-ray diffraction and/or Raman spectroscopy allows a noninvasive analysis of reaction products and phase changes; it is a key technique when studying mechanisms of mechanochemical transformations.[52−57] Ball-milling reactions monitored *in situ* by PXRD revealed three aspects: (1) the nature of the solvent

DOI: 10.1021/acs.cgd.7b01436
Cryst. Growth Des. 2018, 18, 954−961

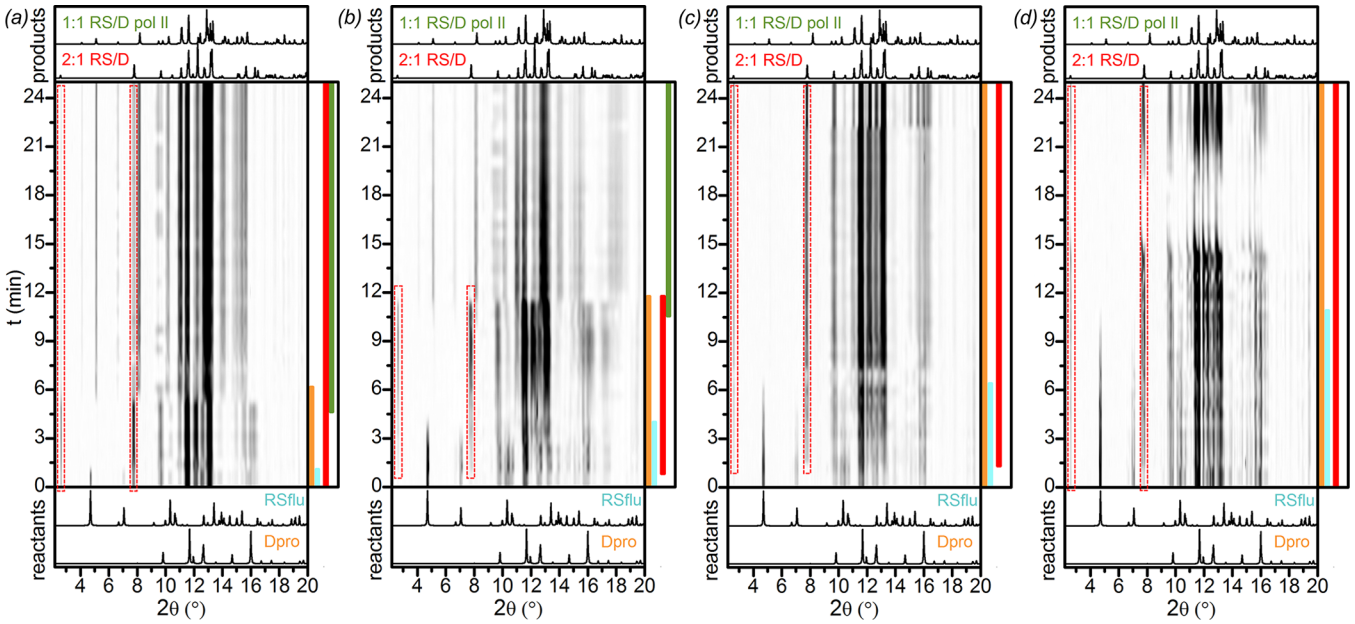

Figure 4. *In situ* ball-milling PXRD patterns for the **RS/D** system, 1:1 ratio, λ = 1 Å: (a) MeOH-, (b) EtOH-, (c) ISPN-, and (d) ACN-LAG. Colored bands on the right side of each image represent the presence of phases; red dashed line indicates two the most representative peaks of the 2:1 phase.

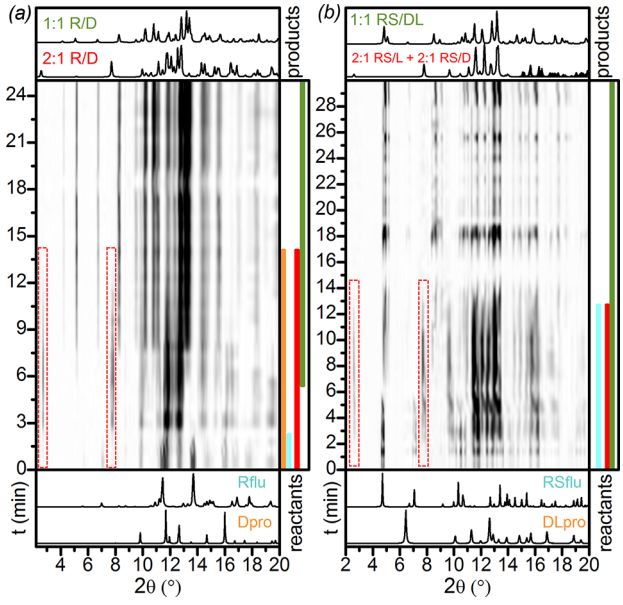

Figure 5. *In situ* ball-milling PXRD patterns (1:1 ISPN-LAG, λ = 1 Å) for (a) the **R/D** system and (b) the **RS/DL** system. Colored bands on the right side of each image represent the presence of phases; red dashed line indicates two the most representative peaks of the **2:1** phase.

Scheme 2. Structural Types in the flu/pro System

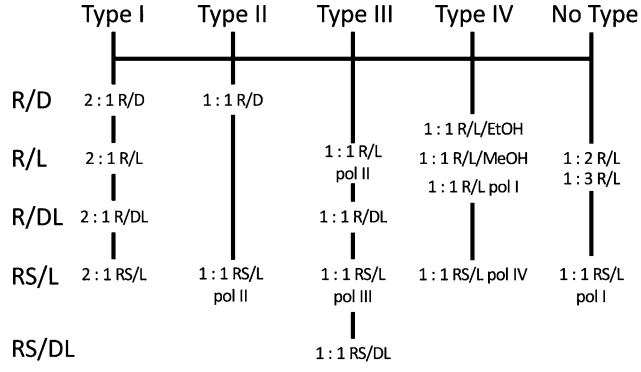

significantly affects the reaction rate and occasionally the reaction pathway; (2) the **2:1** phase is the intermediate product on the way to the **1:1** phase; and (3) the (**2:1 RS/L** + **2:1 RS/D**) conglomerate is a coproduct in the **RS/DL** system. The examples illustrating each of the aforementioned statements are given below.

(1) In all 1:1 LAG experiments of the **R/L** system, the reaction starts with the formation of the **2:1** phase followed by the emergence of a second phase: MeOH-LAG results in the **1:1 R/L/MeOH** cocrystal solvate; EtOH-LAG (and ISPN-LAG) leads to a mixture of the **2:1** and **1:3 R/L** phases, and ACN-LAG to a mixture of the **2:1** and **1:2 R/L** phases (Figure 3). The **2:1** phase thus seems kinetically favored under these conditions, and substantial amounts of it remain in the resultant powders after ACN-, EtOH-, and ISPN-LAG reactions. The nature of the solvent also affected significantly the reaction rate, which was particularly seen in the **RS/D** system: ACN- and ISPN-LAG in most cases stopped at the **2:1 RS/D** phase as compared to MeOH- and EtOH-LAG in which the **2:1** phase converted into the **1:1 RS/L pol II** phase (Figure 4).

(2) A stepwise mechanism of cocrystal formation has been already reported for the glycine/oxalic acid system;[58] another example reported by Coquerel et al. presents a stepwise polymorphic transformation of racemic modafinil.[59] With respect to **flu/pro** system, the emergence of the **2:1** phase as an intermediate product in the 1:1 grinding reactions can be illustrated by the **R/D** system (Figure 5a): the reaction starts with the formation of the **2:1 R/D** phase which as the reaction proceeds converts into the **1:1 R/D** phase. This result is in agreement with

DOI: 10.1021/acs.cgd.7b01436
Cryst. Growth Des. 2018, 18, 954−961

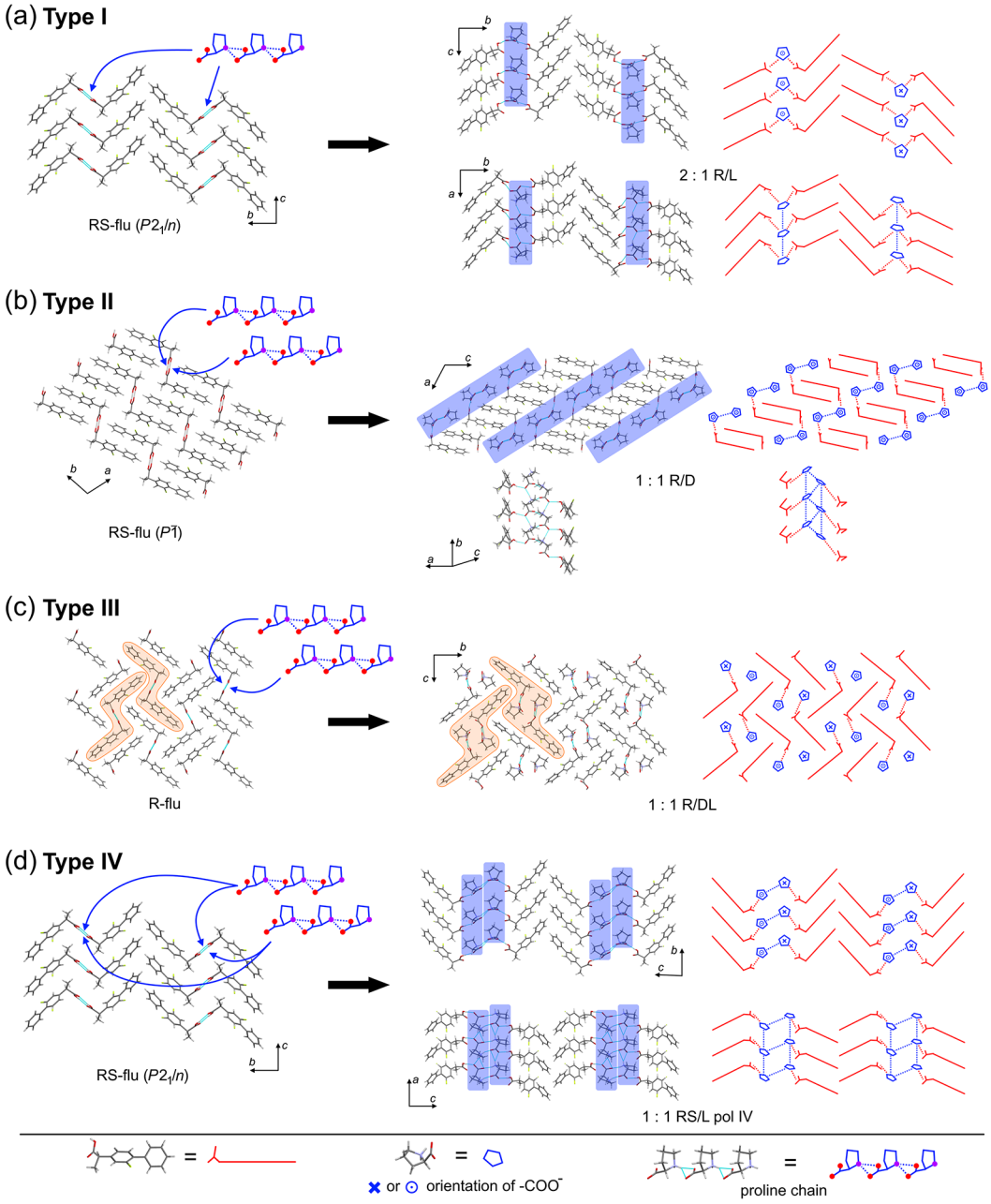

Figure 6. (a–d) Representation of the four packing types distinguished for the **flu**/**pro** cocrystals. Blue-shaded areas indicate **pro** layers formed by **pro** chains "wedged" into **flu** dimers; orange-shaded areas highlight similar block-type structural motifs found in pure **flu** and its cocrystal – **pro** chains again are "wedged" into **flu** dimers.

our preliminary step-by-step experiments: 2:1 LAG results in the **2:1 R/D** form; the **2:1** samples reground with an equimolar amount of D-**pro** yield the **1:1** form; the latter can be obtained directly by the 1:1 ratio LAG (Figure S2.20).

(3) The formation of the conglomerate as a coproduct in the **RS/DL** system can be illustrated by the 1:1 ISPN-LAG (Figure 5b): the (**2:1 RS/L** + **2:1 RS/D**) conglomerate appears within the first minutes of reaction and completely disappears after 14 min. The 2:1 LAG in the **RS/DL** system also yields the conglomerate, often as a coproduct of the **1:1 RS/DL** phase (Figure S2.43c,d).

The solvent's influence on LAG can most likely be associated with the solution behavior of both compounds.[60] **Flu** and **pro** reach the best solubility in MeOH and EtOH, and thus reactions in the presence of these solvents proceed faster typically yielding pure products. Even though **flu** is soluble in ACN and ISPN, **pro** is almost insoluble in these solvents, which may explain why the reactions proceed more slowly. Added liquid might facilitate diffusion of molecules from the reactant to the product phase via solution phase.[61,62] The rate of diffusion depends on the solubility and increases with grinding as it is inversely proportional to the particle size.

Determined cocrystal structures can be grouped into four packing types. Depending on the combination, a particular system can adopt one or several packing types (Scheme 2). A detailed structural analysis is given in Supporting Information.

Pro zwitterions in the cocrystals keep forming infinite head-to-tail chains via strong charge-assisted N–H···O hydrogen

DOI: 10.1021/acs.cgd.7b01436
Cryst. Growth Des. 2018, 18, 954–961

bonds, typical of amino acid crystals. In its cocrystals, **flu** tends to pertain the packing arrangement as in the pure compound with **pro** chains wedged in between. In the cocrystals of packing types I and IV, **flu** is arranged similarly to ***RS*-flu** ($P2_1/n$); the cocrystals with the type II packing resemble ***RS*-flu** ($P\bar{1}$), and the cocrystals of type III have **flu** packed as in ***R*-flu**. This observation indicates that the interactions between **flu** molecules contribute significantly to the overall structure, providing the most favorable molecular arrangement (Figure 6).

Cocrystals with the **1:2** and **1:3** stoichiometries found for the **R/L** system (Figure S2.54) represent an extremely rare case when a coformer prefers connecting to itself rather than to its partner; thus, **flu** is linked to only one of the **pro** molecules. These two examples highlight that strong charge-assisted hydrogen bonds are highly competitive with other interactions in the overall packing.

CONCLUSIONS

Herein we showed a level of complexity that can be reached when working with two chiral coformers, producing in total 17 new cocrystals. LAG proved highly efficient as an alternative to conventional crystallization techniques, providing crystal forms that were not easily accessible from solution. *In situ* ball-milling confirmed that the **2:1** cocrystals are the most kinetically favorable and emerge first during grinding. A stepwise mechanism was suggested for the formation of several **1:1** cocrystals, with the **2:1** phase being converted into the **1:1** as reaction proceeds. The choice of solvent for LAG was found to be important as it affected the reaction rate and occasionally the reaction pathway. *In situ* PXRD collected upon varied temperature revealed additional cocrystals that emerged at higher temperatures and a phase crossover.

The complexity in the **flu/pro** system seems to be associated not only with the distinctive molecular features of the initial compounds, e.g., the conformational flexibility of **pro**, but also with chirality. The possibility of cocrystal formation between chiral entities highly depend on how their three-dimensional structures "suit" one another. Thus, we can expect that some combinations of the chiral coformers may be more favorable than others, which may even result in an enantiospecific behavior—when only one of the enantiomers forms a cocrystal.[7,9] Introducing racemic compounds to the system may result in even more efficient packing as, with more chiral centers at hand, the system has more possibilities to find a better molecular arrangement in comparison with the pairs of pure enantiomers: thus, **1:1 RS/DL** cocrystal has the highest melting point, which may indicate a more efficient packing with stronger interactions.

The fundamental insight into various aspects of cocrystallization gained via studying **flu/pro** system can serve as a blueprint when designing and developing cocrystals with zwitterionic coformers for industrial applications. Knowing how to combine various state-of-the-art characterization methods provides a benchmark to tackle complex problems related not only to cocrystallization but also to other solid-state fields.

ASSOCIATED CONTENT

Supporting Information

The Supporting Information is available free of charge on the ACS Publications website at DOI: 10.1021/acs.cgd.7b01436.

Extensive experimental section as well as additional results and discussion for each **flu/pro** combination (PDF)

Accession Codes

CCDC 1537401−1537422 contain the supplementary crystallographic data for this paper. These data can be obtained free of charge via www.ccdc.cam.ac.uk/data_request/cif, or by emailing data_request@ccdc.cam.ac.uk, or by contacting The Cambridge Crystallographic Data Centre, 12 Union Road, Cambridge CB2 1EZ, UK; fax: +44 1223 336033.

AUTHOR INFORMATION

Corresponding Authors

*(T.L.) E-mail: tom.leyssens@uclouvain.be.
*(F.E.) E-mail: franziska.emmerling@bam.de.

ORCID

Nikolay Tumanov: 0000-0001-6898-9036
Geoffroy Hautier: 0000-0003-1754-2220
Franziska Emmerling: 0000-0001-8528-0301

Notes

The authors declare no competing financial interest.

ACKNOWLEDGMENTS

The authors thank UCL, FNRS, FRIA (scholarship allocated to N.T.), and COST Action (CM1402) for the financial support; PC2 platform (UNamur) for the equipment; ESRF, PSI, and BESSY II for the beam time; Dr. D. Waroquiers, Dr. G. Yu, Prof. R. Cerny, Prof. J. van de Streek, L. Baulard, and P. Van Velthem for their help and advice; and CISM/UCL and CÉCI for providing computational resources.

ABBREVIATIONS

PXRD, powder X-ray diffraction; flu, flurbiprofen; pro, proline; MeOH, methanol; EtOH, ethanol; ISPN, isopropanol; ACN, acetonitrile; DFT, density functional theory

REFERENCES

(1) Shan, N.; Zaworotko, M. J. *Drug Discovery Today* **2008**, *13*, 440−446.
(2) Schultheiss, N.; Newman, A. *Cryst. Growth Des.* **2009**, *9*, 2950−2967.
(3) Aakeröy, C. B.; Salmon, D. J. *CrystEngComm* **2005**, *7*, 439−448.
(4) Bučar, D.-K. *Cryst. Growth Des.* **2017**, *17*, 2913−2918.
(5) Aakeröy, C. B.; Forbes, S.; Desper, J. *J. Am. Chem. Soc.* **2009**, *131*, 17048−17049.
(6) Aitipamula, S.; Chow, P. S.; Tan, R. B. H. *CrystEngComm* **2014**, *16*, 3451−3465.
(7) Friščić, T.; Jones, W. *Faraday Discuss.* **2007**, *136*, 167−178.
(8) Eddleston, M. D.; Arhangelskis, M.; Friščić, T.; Jones, W. *Chem. Commun.* **2012**, *48*, 11340−11342.
(9) Springuel, G.; Leyssens, T. *Cryst. Growth Des.* **2012**, *12*, 3374−3378.
(10) Chow, S. F.; Chen, M.; Shi, L.; Chow, A. H. L.; Sun, C. C. *Pharm. Res.* **2012**, *29*, 1854−1865.
(11) Bien, J. T.; Deshpande, P. P.; Dimarco, J. D.; Gougoutas, J. Z.; Grosso, J. A.; Lai, C.; Lobinger, H.; Nirschl, A. A.; Ramakrishnan, S.; Riebel, P.; Singh, J.; Chenchi, W. Patent WO 2008/002824A1. EP2069374A1, 2008.
(12) Tilborg, A.; Springuel, G.; Norberg, B.; Wouters, J.; Leyssens, T. *CrystEngComm* **2013**, *15*, 3341−3350.
(13) Deshpande, P. P.; Singh, J.; Pullockaran, A.; Kissick, T.; Ellsworth, B. A.; Gougoutas, J. Z.; Dimarco, J.; Fakes, M.; Reyes, M.; Lai, C.; Lobinger, H.; Denzel, T.; Ermann, P.; Crispino, G.; Randazzo, M.; Gao, Z.; Randazzo, R.; Lindrud, M.; Rosso, V.; Buono, F.;

DOI: 10.1021/acs.cgd.7b01436
Cryst. Growth Des. 2018, 18, 954−961

Doubleday, W. W.; Leung, S.; Richberg, P.; Hughes, D.; Washburn, W. N.; Meng, W.; Volk, K. J.; Mueller, R. H. *Org. Process Res. Dev.* **2012**, *16*, 577−585.
(14) Ramanathan, C. R.; Periasamy, M. *Tetrahedron: Asymmetry* **1998**, *9*, 2651−2656.
(15) Shyam Sundar, M.; Talele, H. R.; Mande, H. M.; Bedekar, A. V.; Tovar, R. C.; Muller, G. *Tetrahedron Lett.* **2014**, *55*, 1760−1764.
(16) Hu, X.; Shan, Z.; Chang, Q. *Tetrahedron: Asymmetry* **2012**, *23*, 1327−1331.
(17) Timofeeva, T. V.; Kuhn, G. H.; Nesterov, V. V.; Nesterov, V. N.; Frazier, D. O.; Penn, B. G.; Antipin, M. Y. *Cryst. Growth Des.* **2003**, *3*, 383−391.
(18) Qu, X.; Lu, J.; Zhao, C.; Boas, J. F.; Moubaraki, B.; Murray, K. S.; Siriwardana, A.; Bond, A. M.; Martin, L. L. *Angew. Chem., Int. Ed.* **2011**, *50*, 1589−1592.
(19) Aakeröy, C. B.; Bahra, G. S.; Brown, C. R.; Hitchcock, P. B.; Patell, Y.; Seddon, K. R.; Bao-Sheng, L. *Acta Chem. Scand.* **1995**, *49*, 762−767.
(20) Subha Nandhini, M.; Krishnakumar, R. V.; Natarajan, S. *Acta Crystallogr., Sect. C: Cryst. Struct. Commun.* **2001**, *57*, 423−424.
(21) Fu, T. Y.; Scheffer, J. R.; Trotter, J. *Acta Crystallogr., Sect. C: Cryst. Struct. Commun.* **1997**, *53*, 1259−1262.
(22) Anitha, K.; Athimoolam, S.; Natarajan, S. *Acta Crystallogr., Sect. C: Cryst. Struct. Commun.* **2006**, *62*, o567−o570.
(23) Athimoolam, S.; Natarajan, S. *Acta Crystallogr., Sect. C: Cryst. Struct. Commun.* **2007**, *63*, o283−o286.
(24) Min Jin, Z.; Jiang Pan, Y.; Lin Hu, M.; Shen, L.; Chao Li, M. *Cryst. Res. Technol.* **2003**, *38*, 1009−1012.
(25) Tilborg, A.; Leyssens, T.; Norberg, B.; Wouters, J. *Cryst. Growth Des.* **2013**, *13*, 2373−2389.
(26) Prasad, G. S.; Vijayan, M. *Acta Crystallogr., Sect. B: Struct. Sci.* **1993**, *49*, 348−356.
(27) Thukral, K.; Vijayan, N.; Singh, B.; Bdikin, I.; Haranath, D.; Maurya, K. K.; Philip, J.; Soumya, H.; Sreekanth, P.; Bhagavannarayana, G. *CrystEngComm* **2014**, *16*, 9245−9254.
(28) Hernández-Paredes, J.; Olvera-Tapia, A. L.; Arenas-García, J. I.; Höpfl, H.; Morales-Rojas, H.; Herrera-Ruiz, D.; Gonzaga-Morales, A. I.; Rodríguez-Fragoso, L. *CrystEngComm* **2015**, *17*, 5166−5186.
(29) Rogowska, P.; Cyrański, M. K.; Sporzyński, A.; Ciesielski, A. *Tetrahedron Lett.* **2006**, *47*, 1389−1393.
(30) Flippen, J. L.; Gilardi, R. D. IUCr. *Acta Crystallogr., Sect. B: Struct. Crystallogr. Cryst. Chem.* **1975**, *31*, 926−928.
(31) Macrae, C. F.; Bruno, I. J.; Chisholm, J. A.; Edgington, P. R.; McCabe, P.; Pidcock, E.; Rodriguez-Monge, L.; Taylor, R.; van de Streek, J.; Wood, P. A. *J. Appl. Crystallogr.* **2008**, *41*, 466−470.
(32) Kayushina, R. L.; Vainshtein, B. K. *Kristallografiya* **1965**, *10*, 833 (In Russian).
(33) Janczak, J.; Luger, P. *Acta Crystallogr., Sect. C: Cryst. Struct. Commun.* **1997**, *53*, 1954−1956.
(34) Myung, S.; Pink, M.; Baik, M. H.; Clemmer, D. E. *Acta Crystallogr., Sect. C: Cryst. Struct. Commun.* **2005**, *61*, 506−508.
(35) Hayashi, Y.; Matsuzawa, M.; Yamaguchi, J.; Yonehara, S.; Matsumoto, Y.; Shoji, M.; Hashizume, D.; Koshino, H. *Angew. Chem., Int. Ed.* **2006**, *45*, 4593−4597.
(36) Padmanabhan, S.; Suresh, S.; Vijayan, M. *Acta Crystallogr., Sect. C: Cryst. Struct. Commun.* **1995**, *51*, 2098−2100.
(37) Grzesiak, A. L.; Matzger, A. J. *J. Pharm. Sci.* **2007**, *96*, 2978−2986.
(38) Allen, F. H. *Acta Crystallogr., Sect. B: Struct. Sci.* **2002**, *58*, 380−388.
(39) Hammersley, A. P.; Svensson, S. O.; Hanfland, M.; Fitch, A. N.; Hausermann, D. *High Pressure Res.* **1996**, *14*, 235−248.
(40) Hinrichsen, B.; Dinnebier, R. E.; Jansen, M. *Commission on Powder Diffraction. Hrsg.: Int. Union of Crystallography Newsletter* **2005**, 12−22.
(41) Bertani, P.; Raya, J.; Bechinger, B. *Solid State Nucl. Magn. Reson.* **2014**, *61*−*62*, 15−18.
(42) Solomos, M. A.; Mohammadi, C.; Urbelis, J. H.; Koch, E. S.; Osborne, R.; Usala, C. C.; Swift, J. A. *Cryst. Growth Des.* **2015**, *15*, 5068−5074.
(43) Wahl, H.; Haynes, D. A.; Le Roex, T. *South African J. Chem.* **2016**, *69*, 35−43.
(44) Bučar, D.-K.; Day, G. M.; Halasz, I.; Zhang, G. G. Z.; Sander, J. R. G.; Reid, D. G.; MacGillivray, L. R.; Duer, M. J.; Jones, W. *Chem. Sci.* **2013**, *4*, 4417.
(45) Görbitz, C. H. *Crystallogr. Rev.* **2015**, *21*, 160−212.
(46) Friščić, T. *Chem. Soc. Rev.* **2012**, *41*, 3493−3510.
(47) Hernández, J. G.; Bolm, C. *J. Org. Chem.* **2017**, *82*, 4007−4019.
(48) James, S. L.; Adams, C. J.; Bolm, C.; Braga, D.; Collier, P.; Friščić, T.; Grepioni, F.; Harris, K. D. M.; Hyett, G.; Jones, W.; Krebs, A.; Mack, J.; Maini, L.; Orpen, G.; Parkin, I. P.; Shearouse, W. C.; Steed, J. W.; Waddell, D. C. *Chem. Soc. Rev.* **2012**, *41*, 413−447.
(49) Braga, D.; Maini, L.; Grepioni, F. *Chem. Soc. Rev.* **2013**, *42*, 7638−7648.
(50) Métro, T.; Salom-Roig, X. J.; Reverte, M.; Martinez, J.; Lamaty, F. *Green Chem.* **2015**, *17*, 204−208.
(51) Ravnsbaek, D.; Filinchuk, Y.; Cerenius, Y.; Jakobsen, H. J.; Besenbacher, F.; Skibsted, J.; Jensen, T. R. *Angew. Chem., Int. Ed.* **2009**, *48*, 6659−6663.
(52) Halasz, I.; Puškarić, A.; Kimber, S. a J.; Beldon, P. J.; Belenguer, A. M.; Adams, F.; Honkimäki, V.; Dinnebier, R. E.; Patel, B.; Jones, W.; Strukil, V.; Friščić, T. *Angew. Chem., Int. Ed.* **2013**, *52*, 11538−11541.
(53) Gracin, D.; Strukil, V.; Friščić, T.; Halasz, I.; Užarević, K. *Angew. Chem., Int. Ed.* **2014**, *53*, 6193−6197.
(54) Užarević, K.; Halasz, I.; Friščić, T. *J. Phys. Chem. Lett.* **2015**, *6*, 4129−4140.
(55) Fischer, F.; Heidrich, A.; Greiser, S.; Benemann, S.; Rademann, K.; Emmerling, F. *Cryst. Growth Des.* **2016**, *16*, 1701−1707.
(56) Batzdorf, L.; Fischer, F.; Wilke, M.; Wenzel, K.-J.; Emmerling, F. *Angew. Chem., Int. Ed.* **2015**, *54*, 1799−1802.
(57) Fischer, F.; Lubjuhn, D.; Greiser, S.; Rademann, K.; Emmerling, F. *Cryst. Growth Des.* **2016**, *16*, 5843−5851.
(58) Tumanov, I. A.; Achkasov, A. F.; Boldyreva, E. V.; Boldyrev, V. V. *CrystEngComm* **2011**, *13*, 2213−2216.
(59) Linol, J.; Morelli, T.; Petit, M.-N.; Coquerel, G. *Cryst. Growth Des.* **2007**, *7*, 1608−1611.
(60) Belenguer, A. M.; Lampronti, G. I.; Cruz-Cabeza, A. J.; Hunter, C. A.; Sanders, J. K. M. *Chem. Sci.* **2016**, *7*, 6617−6627.
(61) Bowmaker, G. A. *Chem. Commun.* **2013**, *49*, 334−348.
(62) Boldyreva, E. *Chem. Soc. Rev.* **2013**, *42*, 7719−7738.

DOI: 10.1021/acs.cgd.7b01436
Cryst. Growth Des. 2018, 18, 954−961